Simulation of the transmission and time of flight properties of the KATRIN main spectrometer

Bachelorarbeit Physik

Oliver Ledwig

July 2013

Institut für Kernphysik
Mathematisch-Naturwissenschaftliche Fakultät
Westfälische Wilhelms-Universität Münster

Contents

1 Introduction

The Neutrino is one of the fundamental particles which make up the universe, but it is also still one of the least understood. The Karlsruhe TRItium Neutrino (KATRIN) experiment will investigate the most important open issue in neutrino physics, the question of the absolute mass scale for neutrinos. This will be accomplished in a a model-independent way by investigating the kinematics of electrons from beta decay. Previous experiments have given an upper limit to the electron anti-neutrino mass of 2.3 eV, KATRIN will either improve this limit by one order of magnitude down to 0.2 eV (90% CL), or discover the actual mass, if it is larger than 0.35 eV. This requires an improvement by two orders of magnitude with respect to accuracy.

In this thesis, measurements for the KATRIN main spectrometer concerning transmission and time of flight properties were examined. This was done by simulating the experimental conditions with the Kassiopeia toolkit, and comparing the results of the simulation with the ones obtained by the measurements. This comparison can help to verify the experimental results or find shortcomings in the experimental setup.

2 Neutrinos

In the beginning of the 20th century, physicists developed the modern view of the atom, consisting of a dense nucleus and an electron cloud. In 1932 it became evident that nuclei are made up of protons and neutrons. In 1930 a fourth particle, the neutrino was added to the list of elementary particles, which before consisted only of electron, proton, and neutron. This was done in order to reconcile the beta decay with the conservation laws for energy, momentum and angular momentum. It was Pauli who suggested that the missing energy in the β-decay might be carried off by a neutral particle, which had to be very hard to detect and was at first assumed to be massless. The first experimental evidence for neutrinos was found in 1956 in the Cowan–Reines neutrino experiment, where an uncharged subatomic particle with very low mass was observed, the electron antineutrino $\bar{\nu}_e$.

Starting in the late 1960s, various experiments found much lower flux rates of solar neutrinos than predicted by the standard model, which assumed that neutrinos are massless. The same effect was later observed with atmospheric neutrinos. The discrepancies could be resolved by postulating a non-zero neutrino mass, which allows the neutrinos to change flavors when propagating with time. With this model, the experimental flux rates from solar neutrinos could be explained well. These neutrino oscillations could later also be measured in reactor- and particle accelerators experiments, which in sum provides strong evidence, that neutrinos have non-zero masses. Unfortunately neutrino oscillation experiments are not sensitive to neutrino masses directly, as they can only measure the neutrino mass splitting. Hence, other methods have to be used to find the absolute neutrino mass scale, such as the neutrinoless double beta decay, cosmological neutrino mass studies, or model-independent experiments like KATRIN.

3 The KATRIN Experiment

The KATRIN experiment is a direct neutrino mass experiments, which aims to detect the electron neutrino mass with a sensitivity of 200 meV at 90% C.L. by investigating the kinematics of the β^--Decay of ^{3}H. KATRIN measures the endpoint region of the β-decay spectrum of tritium, which is mainly a function of m_{ν_e}. The tritium spectrum is shown in figure 1 with the endpoint region plotted for the case of massless, light and heavy neutrinos.

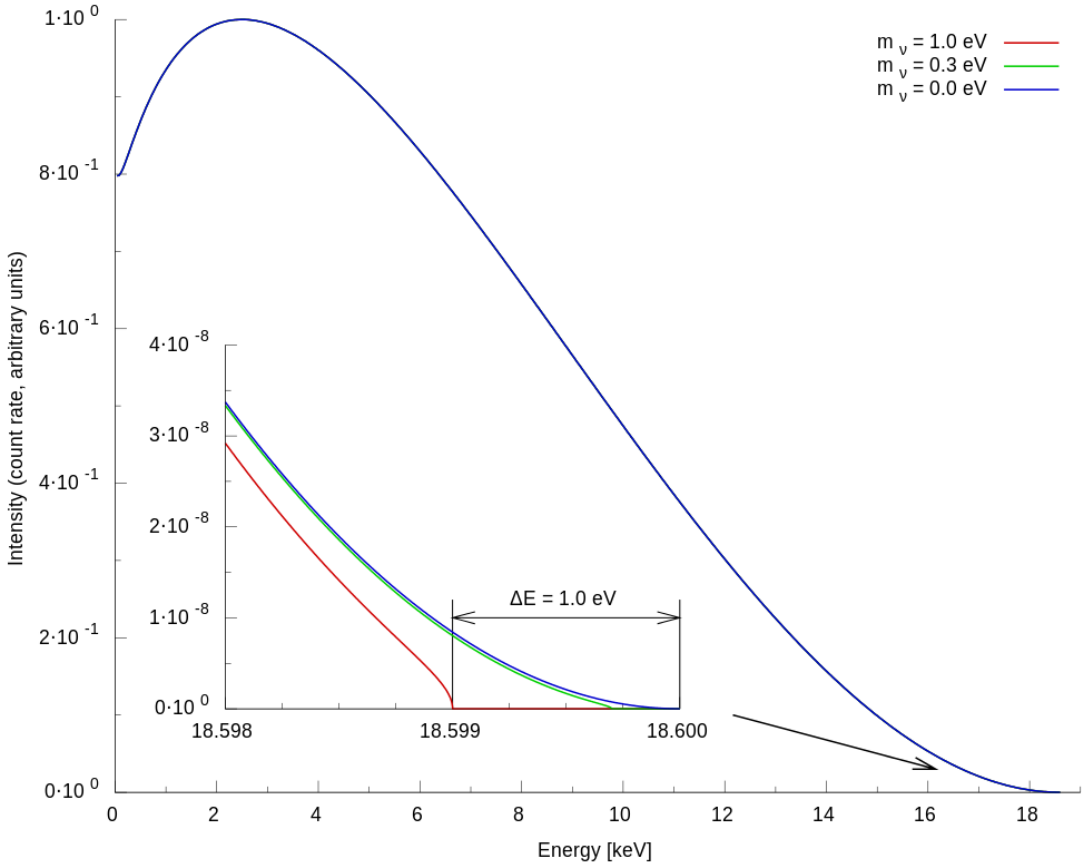

Figure 1: Tritium β-spectrum with zoom into the region close to the endpoint. Figure taken from [Be12].

The 70 m-long experimental setup (see figure 2) consists of:

- A Windowless Gaseous tritium Source (WGTS), where 10^{11} electrons are produced per second by the β-decay of molecular high-purity tritium gas at a temperature of 30 K
- An electron transport and tritium elimination section, where the tritium flow is reduced by more than 14 orders of magnitude
- The electrostatic prespectrometer of MAC-E-Filter type, which offers the option to prefilter the low-energy part of the tritium β- decay spectrum
- The large electrostatic main spectrometer of MAC-E-Filter type which represents the precision energy filter for electrons
- A segmented Si-PIN diode array to count the transmitted electrons

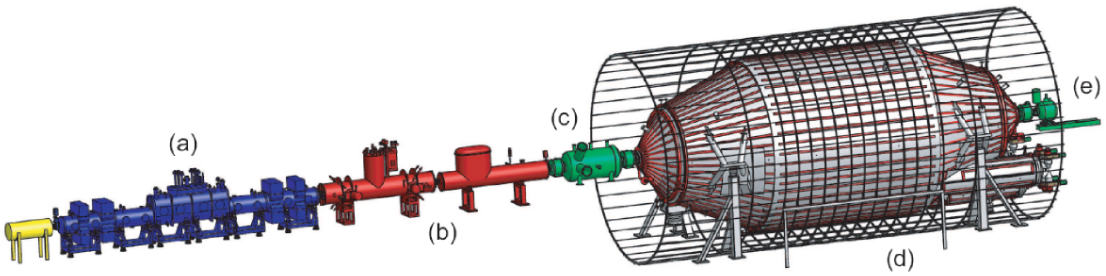

Figure 2: Overview of the KATRIN experiment. (a) windowless gaseous tritium source, WGTS; (b) differential and cryo pumping sections, DPS/CPS; (c) pre-spectrometer, PS; (d) main spectrometer, MS; (e) focal plane detector, FPD. Sections a,b are also called the source-transport-section, STS, while sections c,d,e are called the spectrometer-detector-section, SDS. Figure taken from [KAT04].

3.1 MAC-E-Filter

The main concept behind achieving the high sensitivity of the KATRIN experiment is the **M**agnetic **A**diabatic **C**ollimation combined with an **E**lectrostatic Filter (MAC-E). It was proposed in [Bea80] and combines high luminosity and low background with a high energy resolution.

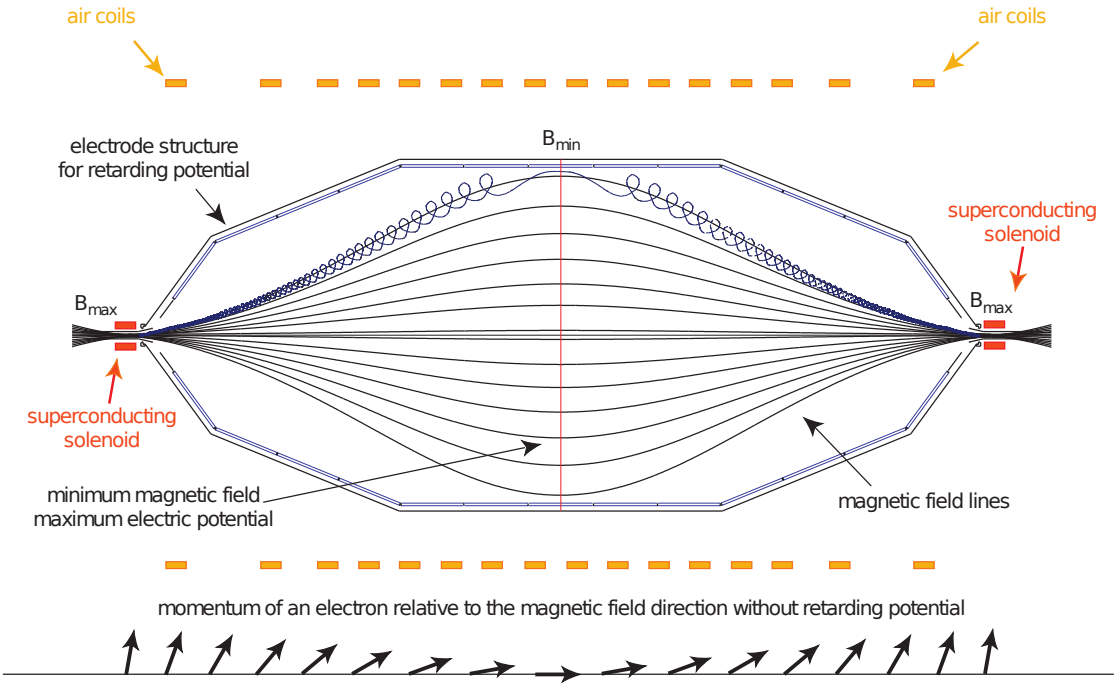

Figure 3: Basic principle of the MAC-E Filter: As a consequence of an adiabatic motion in a inhomogeneous $\vec{B}$-field, the magnetic momentum is conserved which allows a transformation of transversal to longitudinal energy and combined with a electrostatic barrier, energy filtering. Figure taken from [Hug08].

The key features of the MAC-E-Filter are illustrated in figure 3. It consists of two superconducting solenoids, which produce a magnetic guiding field $\vec{B}$, and an electrode system, which creates a retarding potential U_0. Electrons start from the tritium source in the left solenoid with a starting angle to the magnetic field θ_S into the forward hemisphere. They are guided magnetically on a cyclotron motion around the magnetic field lines into the spectrometer, thus resulting in an accepted solid angle of up to 2π. We can decompose the kinetic energy of the electrons at any time as

$$E_{\text{kin}} = E_{\parallel} + E_{\perp} \tag{1}$$

where

$$E_{\perp} = E \sin^2 \theta_S$$

denotes the energy associated with the cyclotron motion and

$$E_{\parallel} = E \cos^2 \theta_S$$

corresponds to longitudinal motion along a magnetic field line. It can be shown, that the magnetic momentum of the electron

$$\mu = \frac{E_{\perp}}{B} \tag{2}$$

is an adiabatic invariant of the motion to all orders in an expansion in ω/ω_c, where ω is the rate of any changes experienced by the particle and

$$\omega_c = \frac{eB}{m}$$

the cyclotron frequency. This means that the magnetic momentum remains nearly constant for changes up to the cyclotron frequency.

As result of this constancy, if B decreases, the transversal energy $E_\perp$ decreases too, and thus according to equation (1) transversal energy can be transformed into longitudinal energy. In the analyzing plane only the longitudinal kinetic energy determines whether an electron can pass the potential barrier U_0, and the remaining transversal energy is not taken into account.

This motivates the design principle of a MAC-E filter: One creates a guiding magnetic field, which drops by multiple orders of magnitude to its minimum value in the analyzing plane in the center of the spectrometer, and an electrostatic potential formed by a system of cylindrical electrodes, which forms an electrostatic barrier in the analyzing plane. In order to achieve an adiabatic motion, the reduction of the magnetic field strength of about four orders of magnitude is extended over a length of about 10 m.

As the widely spread electron beam is transformed into an almost parallel beam in the center of the spectrometer, all electrons with enough energy to pass the electrostatic barrier are reaccelerated and collimated onto a detector, all others are reflected. Therefore the spectrometer acts as a high-energy pass filter. Varying the electrostatic retarding potential allows to measure the beta spectrum $N(E)$ in an integrating mode, meaning that

$$N_{\mathrm{hp,int}}(E) = \int_E^\infty N(E')\mathrm{d}E'$$

can be measured for different energies, which allows the reconstruction of $N(E)$.

To derive the energy resolution of this filter we consider the extreme case, where all of the starting electrons starting energy E^s, is stored in transversal energy $E_\perp^{\mathrm{s}}$. The minimal transversal energy in the analyzing plane $E_\perp^{\mathrm{ap}}$ can be calculated from the constancy of the magnetic momentum according to equation (2) :

$$\begin{aligned} \mu = \frac{E_\perp^{\mathrm{s}}}{B_{\mathrm{max}}} &= \frac{E_\perp^{\mathrm{ap}}}{B_{\mathrm{min}}} = \mathrm{const} \\ \Longrightarrow E_\perp^{\mathrm{ap}} &= E_\perp^{\mathrm{s}} \frac{B_{\mathrm{min}}}{B_{\mathrm{max}}} \,. \end{aligned} \tag{3}$$

Because only the longitudinal energy in the analyzing plane determines whether an electron can pass the electrostatic barrier, and the above equation describes the case where the transversal energy in the analyzing plane is the highest for given total starting energy E^s, we can consider

$$\Delta E = E \frac{B_{\mathrm{min}}}{B_{\mathrm{max}}} \tag{4}$$

as the energy resolution of the ideal MAC-E Filter.

3.2 Transmission function of KATRIN

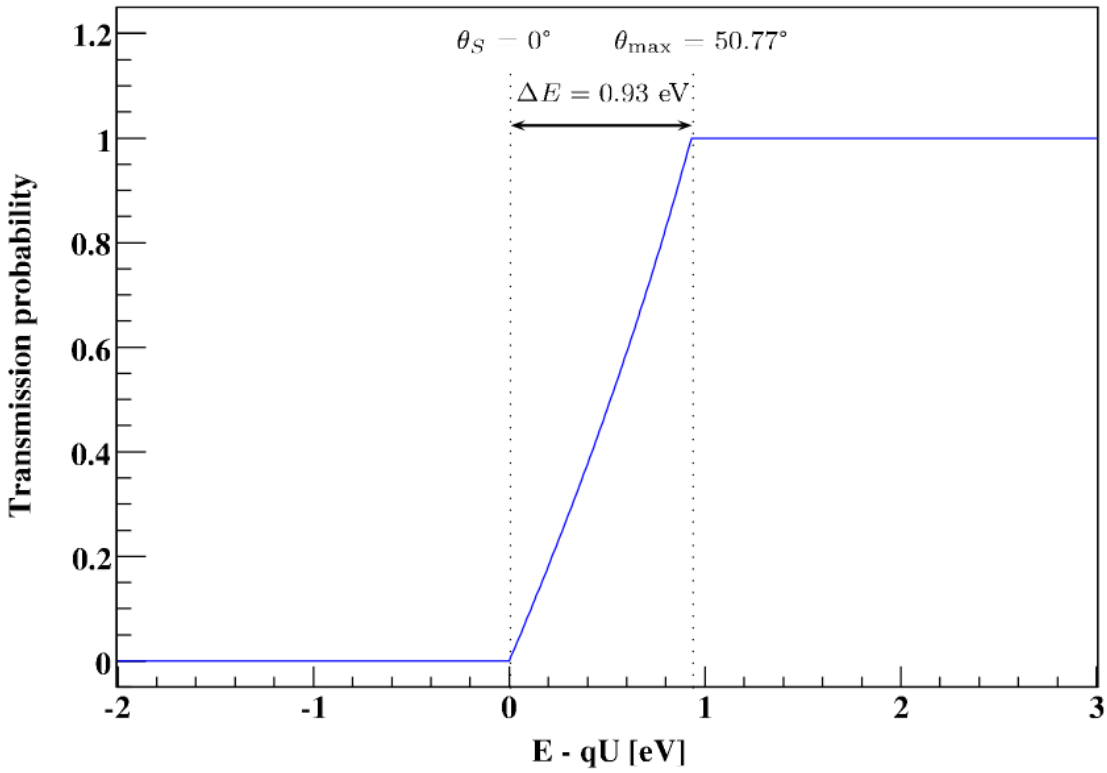

Figure 4: KATRIN Transmission function for electrons with starting energy of 18.6 eV and angles from $\theta_S = 0°$ to $\theta_{max} = 50.77°$ for the standard parameters of the KATRIN experiment ($B_{max} = 6\,T$, $B_{min} = 3 \cdot 10^{-4}\,T$). This setting results in an energy resolution of $\Delta E = 0.93\,keV$. Figure taken from[Wol08].

The transmission function $T(E,U_0)$ describes the relative rate of electrons, which can pass the retarding potential U_0 of the MAC-E Filter. An electron can only pass the analyzing plane, if its longitudinal kinetic energy at the analyzing plane is larger than zero

$$E_{\parallel}^{ap} \geq 0,$$

as the kinetic energy is mostly transformed into longitudinal energy in the analyzing plane, and only this component is relevant for electrons to pass the retarding potential U_0. Together with (1) and (3), the transmission condition can be rewritten as

$$\begin{aligned} 0 \leq E_{\parallel}^{ap} &= E^{ap} - E_{\perp}^{ap} = E^{ap} - E_{\perp}^{s} \frac{B_{min}}{B_{max}} \\ &= E^{s} - qU_0 - E^{s} \sin^2 \theta_S \frac{B_{min}}{B_{max}}. \end{aligned}$$

This means, that only electrons with

$$\theta_{\mathrm{S}} \leq \theta_{\max} = \arcsin \sqrt{\frac{E^{\mathrm{s}} - qU_0}{E^{\mathrm{s}}} \frac{B_{\max}}{B_{\min}}}$$

can pass the filter. We consider an isotropic electron source. The transmission rate is then given by the fraction of the solid angle

$$\Omega_{\mathrm{cap}} = 4\pi \sin^2\left(\frac{\theta_{\max}}{2}\right) = 2\pi\left(1 - \cos\theta_{\max}\right).$$

of the spherical cap which corresponds to $\theta_{\max}$ and the solid angle of a full hemisphere $\Omega_{\mathrm{hem}} = 2\pi$:

$$T(E_{\mathrm{s}},U_0) = \frac{\Omega_{\mathrm{cap}}}{\Omega_{\mathrm{hem}}} = 1 - \cos\theta_{\max}$$

Therefore the transmission function $T(E,U_0)$ of the MAC-E-Filter for an isotropically emitting electron source of energy E is

$$T(E_{\mathrm{s}},U_0) = \begin{cases} 0 & E \leq qU_0 \\ 1 - \sqrt{1 - \frac{E_{\mathrm{s}} - qU_0}{E_{\mathrm{s}}} \frac{B_{\max}}{B_{\min}}} & qU_0 < E \leq qU_0 + \Delta E \\ 1 & qU_0 + \Delta E \leq E \end{cases} \tag{5}$$

This transmission function is shown in figure 4 for the standard KATRIN settings.

3.3 MAC-E TOF measurements

Instead of using the integrating filter mode of a MAC-E Filter, *time of flight (MAC-E-TOF) spectroscopy* [TOF13] can be used to measure the neutrino mass. Essentially, this means measuring the time of flight (TOF) distribution of electrons flying through the MAC-E filter as a function of the kinetic energy and the emission angle. As the kinetic energies depend mainly on the beta spectrum, it can be reconstructed from these measurements, thus providing $m^2_{\nu_e}$. The advantages over the filter mode are:

- TOF measurement of beta electrons passing through a MAC-E-Filter will be very sensitive to subtle energy differences just above the retarding energy, because electrons close to this energy are significantly slowed down. This allows to measure electron energy differences even below the resolution of the MAC-E-Filter, which is $\Delta E = 0.93\,\mathrm{eV}$ for 18.5 keV electrons in case of KATRIN, given a sufficient time resolution.
- The standard MAC-E mode measures only the count rate for each retarding energy, as described above. In contrast, the TOF spectroscopy mode measures the TOF for each decay electron. Thus a full TOF spectrum, sensitive to $m^2_{\nu_e}$, is obtained for each retarding energy. For suitable measurement conditions, this gain of information improves the statistics.

Time of flight measurements are also useful for testing the MAC-E filter, because they turn it into a band-pass, thus allowing more detailed and faster characterization of its transmission properties.

The time of flight can generally be calculated by integrating the reciprocal longitudinal velocity of the electron:

$$\tau(E,\theta) = \int \mathrm{d}z \, \frac{1}{v_{\parallel}}$$

Using the approximation of adiabatic motion and only taking the electric field on the z axis into account, it can then be shown, that the time of flight of an electron emitted in the center of the MAC-E filter at z_{start} and detected at z_{stop} is given by

$$\tau(E,\theta) = \mathrm{d}z \, \frac{E + m_e c^2 - q\Delta U(z)}{\sqrt{p_{\parallel}^2(z)c^2} \cdot c} \, . \tag{6}$$

In figure 5, example time of flight curves are plotted for the KATRIN main spectrometer.

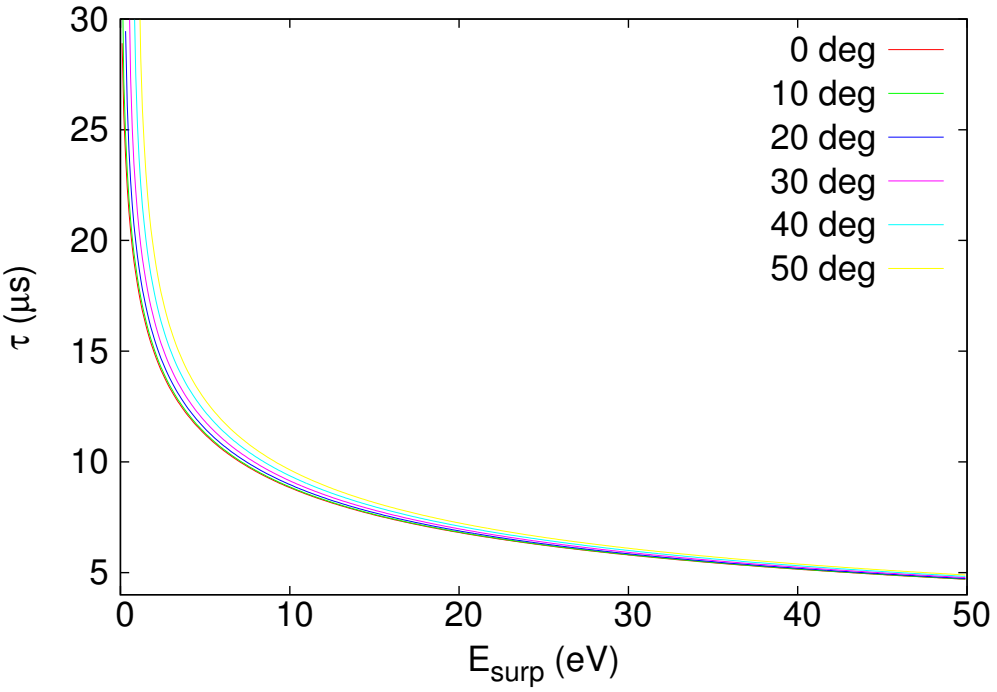

Figure 5: Time-of-flight of a electron in the KATRIN main spectrometer for different starting angles as a function of the surplus energy $E_{\mathrm{surp}} = E - qU$ for a central detector pixel. The starting angle is limited to 50.77 ° due to the KATRIN field design. Figure taken from [TOF13].

3.4 The Main Spectrometer Electron-Gun

The purpose of the electron-gun is to provide electrons with well defined energies and emission angles relative to the magnetic field lines of the KATRIN main spectrometer. It is one of the main tools for commissioning and calibrating the spectrometer. To be able to cover the complete magnetic flux tube of the spectrometer, the electron-gun is attached to a UHV manipulator, so that electrons can be started off the central axis of the spectrometer. This is measured by a horizontal and vertical manipulator angle, which in each case can be set to up to 20°.

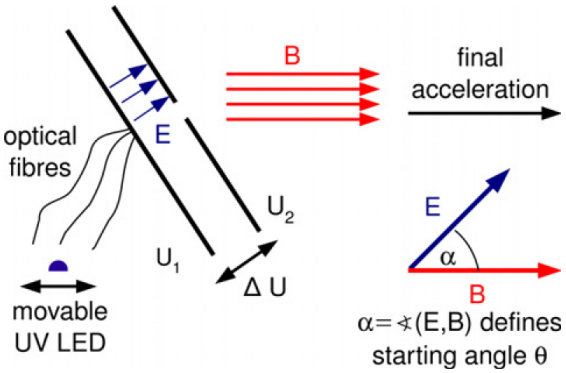

Figure 6: Basic principle of the photoelectron source. Figure taken from [Hug10].

The electrons are emitted from a photocathode surface by irradiation with a UV-LED or laser that can be pulsed (see figure 6). The starting potential is controlled by the E-Gun voltage U_{egun}. From there are accelerated by a strong electric field in a plate capacitor with ΔU non-adiabatically. The angle between the electric field and the magnetic guiding field determines the starting angles of the electrons relative to the $\vec{B}$-field lines and can be chosen by rotation of the plate capacitor or by changing the electric field. As this first acceleration is only done for angle selection, the electrons are further accelerated towards the ground potential in front of the main spectrometer (not shown in figure 6), so that the total kinetic energy gain is qU_{egun}.

4 Kassiopeia

Kassiopeia, which has been developed over the past years by the KATRIN collaboration, is the primary simulation package for the KATRIN Experiment. It is written mainly in C++, and is mainly used for single particle tracking in static electro-magnetic fields. Kassiopeia offers solvers for electric and magnetic fields that use zonal harmonic expansions, when axial symmetric approximations are allowed, and switch to more precise solving methods when needed.
The tracking is done by splitting particle flight paths into discrete steps and then solving the equations of motion for each step.
The parameters of a simulation run, like field geometry, particle start and end conditions, tracking methods, etc. are defined in a XML-like syntax. Physical quantities can be selected to be written to a *ROOT* output file during each step or for each track. There are also "painters" available, which create .vtp files for the *Visualization Toolkit (VTK)*[1] visualizing simulation geometries, particle paths and fields.

4.1 Field Simulation

4.1.1 Magnetic Fields

In Kassiopeia, magnetic fields are computed with the Magfield code, developed by Ferenc Glück. The computation uses elliptic integrals (direct solver), which is slower, but gives precise results even when being inside a coil, or Legendre polynomials (zonal harmonic solver) which is faster and still precise enough for points far away from the coils.

4.1.2 Electric Fields

For electric fields, there are two modules in Kassiopeia:

- The older *Elcd* module was developed by Ferenc Glück at KIT Karlsruhe. Elcd was first implemented as stand-alone module that can compute fields from axially symmetric conical and wire electrodes (Elcd 3.2), and extended later to support arbitrary rectangular and wire electrodes (Elcd 3.3). The disadvantage of this module is, that it needs it owns input files, and cannot use geometries defined for a simulation in the Kassiopeia XML syntax. This means that objects in a simulation, which shall be used as electrodes, but also as geometrical objects, for instance for particle interaction (e.g. starting or terminating surface), have to be defined twice in different formats.

[1] *http://vtk.org/*

- In newer versions, the *KEMField* module was introduced to remove this shortcoming. With this module, objects defined in the more convenient and readable XML syntax can be used both as electrodes or coils and as surface or volume for particle interaction.

Both variants are implemented in Kassiopeia and can be used accordingly. They are both based on the Boundary Element Method described in the next chapter.

4.1.3 Boundary Element Method

The most complex task in particle tracking is finding the electric potential $U(\vec{r})$. One approach to do this for complex electrode geometries, where this cannot be done analytically, is to first discretize all electrodes into simple elements j with a surface charge density σ_j and a Volume V_j. The problem can now be reduced by calculating the individual contribution from each charge sub-element j at the center $\vec{r}_i$ of another segment i:

$$U_{ij} = \int_{\partial V} \mathrm{d}S\, G(\vec{r}_i,\vec{r'})\sigma(\vec{r'}) \tag{7}$$

The integration is carried over the Surface of the element

$$G(\vec{x},\vec{x'}) = -\frac{1}{4\pi\,(\vec{r}-\vec{r'})}$$

is the Green's Function of the three dimensional Laplace-Operator. According to the superposition principle, the total potential U_i at an electrode i is given by the sum over all U_{ij}:

$$U_i = \sum_{j=1}^{N} U_{ij} \tag{8}$$

With discretization, one assumes that the surface charge density $\sigma(\vec{r'})$ is constant across dS'. We can therefore just calculate

$$C_{ij} = \int_{\partial V} dS'\, G(\vec{r}_i,\vec{r'})$$

and write the total potential as

$$U_i = \sum_{j=1}^{N} C_{ij}\sigma_j \tag{9}$$

where σ_j is the charge density of sub-element j. As we know the Potential U_i, and C_{ij} are geometrical factors which can be calculated for given basic geometries like rectangles or triangles, equation (9) is an equation system for the unknown charge density σ_j. Boundary element methods are directed at solving this equation system. In Kassiopeia, elcd uses the Gauß-Jordan algorithm to solve this equation. KEMField introduces the

iterative Robin-Hood algorithm[RH06], which appears to be the most efficient implementation of BEM, both in terms of computation time and memory use, but it is less stable, as there are certain situations where it does not converge.

This algorithm, first sets an initial state, e.g. random or uniformly distributed σ_j. Using this (incorrect) charge configuration, the potential at each sub-element is computed. Of course, the potential across the surface at this point will not be an equipotential because the charge configuration is incorrect. To correct the charge configuration, the two sub-elements with the greatest deviation from the average potential are selected. Then the charges are redistributed such that they are both at the same potential. For the case of two sub-elements, there is an exact solution to the amount of charge that needs to be moved from one element to the other.

The charge exchange propagates its effects to the neighboring elements, allowing the solution to quickly converge. The process is repeated until the maximum difference between the equipotential solution and U_i falls below some pre-determined user-defined threshold.

After the charge densities have been calculated with one of the two described BEM methods, they can be used to compute the resulting potential at an arbitrary point in space by adding up the contributions from all electrode segments. However, the results obtained by this method include the approximation of only taking the center of each electrode segment into account. This emphasizes why a sufficient discretization is needed to produce accurate results, as mentioned earlier.

Furthermore, the algorithm used for computing the resulting potential depends on the type of electrode that is employed, which especially allows to use several approximations when dealing with symmetric geometries. Depending on the needed accuracy and tracking region, The KATRIN main spectrometer can be described as consisting only of axial symmetric electrodes in many cases, which speeds up field computation and tracking time by a considerable amount of time.

5 Simulation of TF and TOF measurements of the main spectrometer

5.1 The energy spread measurements of the main spectrometer

The main objective of this thesis was to simulate the transmission and time of flight properties of the KATRIN main spectrometer. The simulations were based on the KATRIN *E-gun characteristics* measurements, which were proposed in [M313] and performed in July 2013 to commission the electron gun. In these measurements, the main spectrometer vessel was at ground potential, and the inner electrodes were operating at 200 V. The goals of these measurements included testing

- the basic operation mode of the e-gun
- time of flight capability
- the energy resolution of the electron gun.

The simulations were focused on reproducing the time of flight and transmission curves obtained by the measurements M3.A5 and M3.A7 and M4 run 6157 which were performed with the following settings:

	U_{ie} (V)	manip. angle (hor /ver)	Source	puls rate	B_{min}	B_{max}
M3.A5	−200	0°/0°	Laser	100 kHz	5 G	5 T
M3.A7	−200	10°/0°	Laser	100 kHz	5 G	5 T
M4 run 6157	−200	0°/0°	LED	100 kHz	3.8 G	5 T

During these measurements, the E-Gun voltage U_{egun} was swept in a range of about U_{ie} to $U_{\text{ie}} + 80\,\text{V}$. Thus electrons that were accelerated in the E-Gun to a starting energy of $E = eU_{\text{egun}}$ were emitted into the spectrometer and the electron rate of these electrons at the detector were measured. All data off the measurements used in this thesis were either taken from the KATRIN internal elog [SDS13] or retrieved via the BEANS framework, which is a detector analysis logic library included in Kasper (The KATRIN analysis and simulation package), which also contains Kassiopeia.

5.1.1 Measuring the transmission function

Measuring the relative electron rate at the detector as a function of $U_{\text{ie}} - U_{\text{egun}}$ for electron energies in the order of eU_{ie} yields the transmission function of the spectrometer. If the starting energy E is in the order of eU_{ie}, then the transmission width of the spectrometer for energies at about $U_{\text{ie}} = 200\,\text{eV}$ can be easily calculated with equation (4):

$$\Delta E_{\text{mainspec}} = E\frac{B_{\text{min}}}{B_{\text{max}}} \approx 200\,\text{eV} \cdot \frac{5\,\text{G}}{5\,\text{T}} = 0.02\,\text{eV}. \tag{10}$$

Since the E-Gun has an energy line width of $\Delta E_{\text{egun}} = 0.2\,\text{eV}$, which previous measurements showed, the resulting measured transmission function is a convolution of its

energy distribution and the exact spectrometer transmission function equation (5), which for $\Delta E_{\mathrm{egun}} \gg \Delta E_{\mathrm{mainspec}}$ can be regarded as a step function

$$T_{\mathrm{spec}}(E,U_0) = \Theta(E - eU_0)$$

If one assumes, that the energy distribution of the E-Gun is Gaussian around the E-Gun energy E_{egun}:

$$\rho(E,E_{\mathrm{egun}}) = a \exp\left[-\frac{(E - E_{\mathrm{egun}})^2}{2\sigma^2}\right]$$

then the transmission as a function of E_{egun} is given by:

$$\begin{aligned} T_{\mathrm{eff}}(E_{\mathrm{egun}},U_0) &= \int_{-\infty}^{\infty} \rho(E,E_{\mathrm{egun}}) T_{\mathrm{spec}}(E,U_0)\mathrm{d}E \\ &= \int_{-\infty}^{\infty} \exp\left[-\frac{(E - E_{\mathrm{egun}})^2}{2\sigma^2}\right] \Theta(E - eU_0)\mathrm{d}E \\ &= \int_{-\infty}^{-eU_0} \exp\left[-\frac{(E - E_{\mathrm{egun}})^2}{2\sigma^2}\right] \mathrm{d}E \\ &= \int_{-\infty}^{E_{\mathrm{egun}} - eU_0} \exp\left[-\frac{E^2}{2\sigma^2}\right] \mathrm{d}E \end{aligned}$$

We call $E_{\mathrm{egun}} - eU_0$ the surplus energy E_{surp}. The integral is proportional to the so called complementary error function $\mathrm{erfc}(\frac{E_{\mathrm{surp}}}{\sqrt{2}\sigma})$:

$$T_{\mathrm{eff}}(E_{\mathrm{egun}},U_0) = \int_{-\infty}^{E_{\mathrm{surp}}} \exp\left[-\frac{E^2}{2\sigma^2}\right] \mathrm{d}E \propto \mathrm{erfc}(\frac{E_{\mathrm{surp}}}{\sqrt{2}\sigma}) = 1 + \mathrm{erf}\left(\frac{E_{\mathrm{surp}}}{\sqrt{2}\sigma}\right)$$

In fact, in the M3 measurements, it could be shown, that the transmission curve is fit well by this function with $\sigma = 0.134\,\mathrm{eV}$, suggesting that the energy distribution of the E-Gun is approximately Gaussian. In figure 7 one of these fits is shown. It should be noted, that here the transmission rate is plotted against the voltage difference $U_{\mathrm{ie}} - U_{\mathrm{egun}}$. As we assume, that $E_{\mathrm{egun}} = qU_{\mathrm{egun}}$, one could think that this difference is proportional to the surplus energy, but it is not, because U_{ie} is not equal to the retarding potential U_0 in the analyzing plane. U_0 actually depends on the radial position of the electron, and drops from U_{ie} at the electrodes ($r = 4.5\,\mathrm{m}$) to $U_{\mathrm{ie}} - \Delta U$ at the center ($r = 0$). The reason for this is the finite length of the spectrometer, which creates a inhomogeneous electric field with this so called potential penetration of

$$\Delta U = U(r = 0) - U(r = 4.5\,\mathrm{m}) = U(r = 0) - U_{\mathrm{ied}} \approx 2.$$

Therefore, experimental transmission curves (such as in figure 7) are shifted along the x-axis by ΔU.

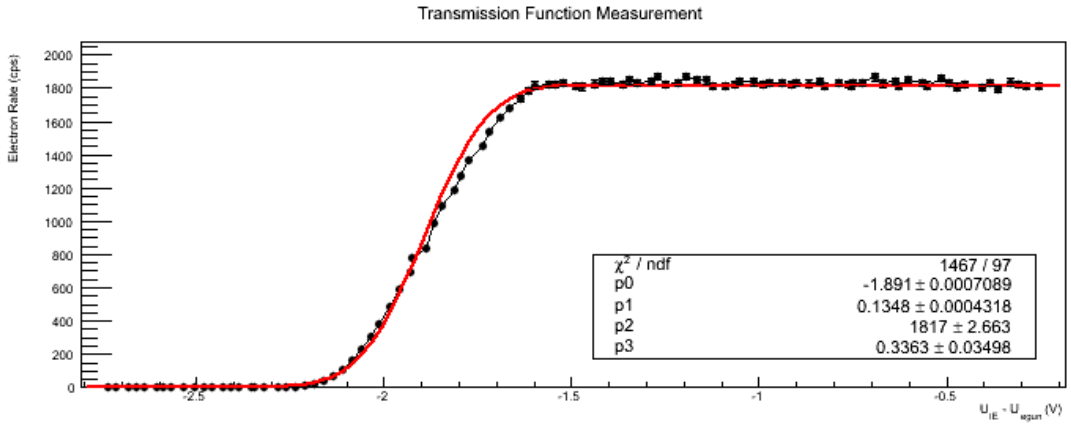

Figure 7: Transmission function of the M3.A05 measurement with the inner electrode at $U_{\mathrm{ie}} = -200\,\mathrm{V}$, and an error function fit. The sigma parameter of the fit function is in the range of 0.132 to 0.135 eV; which is in agreement with the expectation, that the E-gun energy spread dominates the line width.[SDS13]

5.1.2 Measuring the time of flight

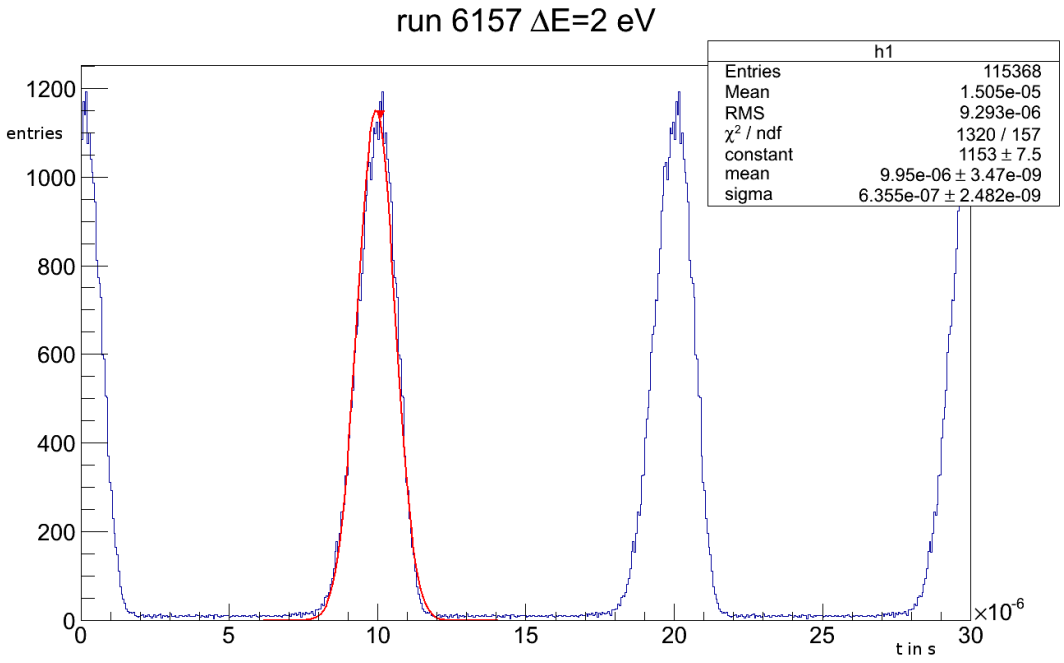

Figure 8: TOF spectrum of m4 run 6157 and a surplus energy of about 2 eV[SDS13]

For flight time measurements of emitted electrons, the UV laser in the E-Gun produces photoelectrons by short (20 ns) triggered UV laser pulses with a repetition rate of at most $f = 100\,\mathrm{kHz}$. To determine time of flight values, one needs a start and stop signal. The start is taken from the pulser of the laser, whereas each detector event serves as stop signal. This signals are fed to a DAQ system. The time of flight is then calculated by the time difference between the detection time and the time of the last detector event.

A TOF spectrum can then be constructed by binning the time of flights into a histogram. This yields peaks with a constant distance of $1/f$, as shown in figure 8. To determine a time of flight value, a peak has to be selected and a mean value has to be determined, e.g. by fitting. Because detector events cannot be mapped to the correct starting event, but only to the last laser pulse, the time of flight values can only be determined up to an unknown offset of $\tau_{\mathrm{off}} = n/f$.

To construct the time of flight curves, TOF spectra are measured as described above as a function of the $U_{\mathrm{IE}} - U_{\mathrm{egun}}$. Then τ is determined for each spectrum, and plotted against the corresponding voltage difference. Due to the described unknown offset τ_{off}, an uncorrected TOF curve contains multiple jumps, which are unphysical (see figure 9), but they can be corrected by applying an offset of $10\,\mu\mathrm{s}$ to the TOF for each jump. A corrected spectrum (see figure 10) then looks similar to figure 5.

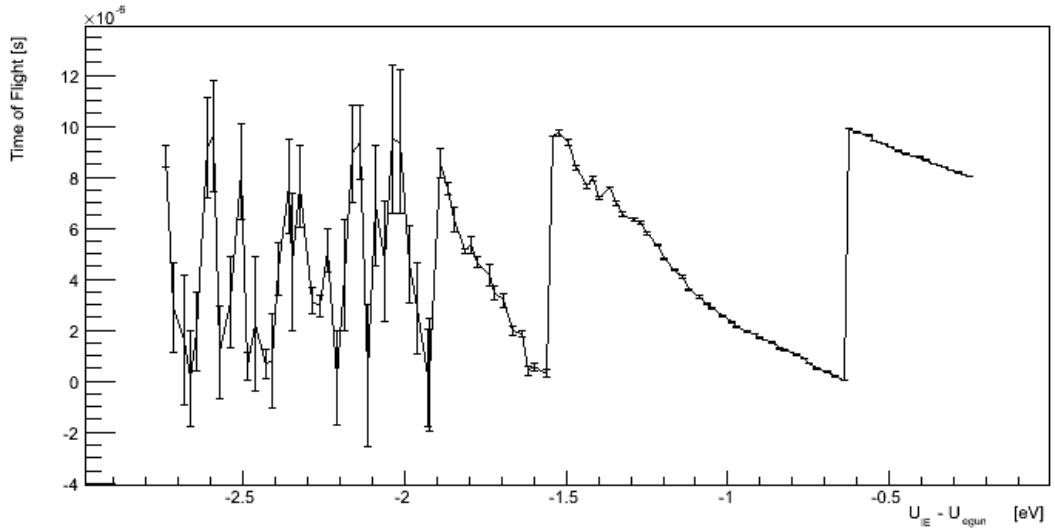

Figure 9: Uncorrected time of flight curve of run 5843 (M3.A07): $U_{\mathrm{IE}} = -200\,\mathrm{V}$, manipulator at 10°h/0°v. Picture taken from [SDS13]

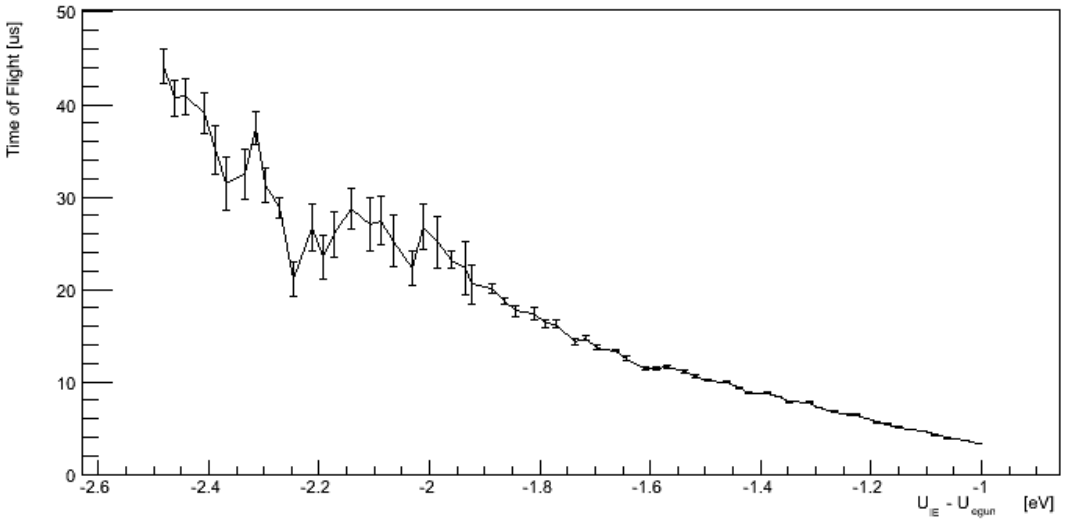

Figure 10: Corrected time of flight curve of run 5843 (M3.A07). The time of flight curves deviates from the expected form as in figure 5 because the electron rate drops for low surplus energies. To obtain more accurate results, the emission rate has to be increased. Picture taken from [SDS13].

5.2 Simulation Settings

The simulations performed for this thesis were intended to emulate the experimental settings described in the previous section and thus verify the transmission function and the time of flight curves reconstructed from this data. The main setup was the following:

- The model of the main spectrometer used for the simulation consists of all important electrodes and coils. For electric fields, it was first tried to use the KEMField zonal harmonic solver, but simulations running with this solver were a lot slower than expected. Therefore the older elcd32 algorithm was tested, which ran significantly faster, thus allowing simulation runs with 1000 particle tracks in about 20 hours. Using the MAF-Cluster ("Münster Analysis Facility"), many of these runs could be run in parallel.
- Magnetic fields were computed using the KEMField zonal harmonic solver.
- A particle generator was used, that starts electrons from a "virtual" starting point in the E-Gun and moves them to the magnets at the entry of the spectrometer, where the actual tracking begins. This means that the flight path and the development of the initial angle distribution of the electron created on the photocatode of the E-Gun is not modeled exactly, instead, they were started inside the magnet at $z = -12.2\,\mathrm{m}$, with a Gaussian energy distribution with $\sigma = 0.134\,\mathrm{eV}$ around the starting energy E with a uniform angle distribution. This is allowed, as the exact starting phase of the electrons (which even highly non adiabatic) is very short and therefore not important for the time of flight.
- Electron trajectories were computed with the adiabatic step solver and an adaptive step size of two times the cyclotron radius [2]. For low surplus energies, adiabatic approximation can be used well, and it was verified that this approximation is precise enough, by assuring that both the relative fluctuations in magnetic momentum and the total energy of the electrons are very low ($< 10^{-6}$)
- Each track was terminated when the electron hit the detector at the end of the spectrometer (transmitted electron) or was reflected (not transmitted).

[2] cyclotron radius: $r_c = \frac{mv_\perp}{|q|B}$.

5.3 Simulation results

5.3.1 Transmission function

Using the settings described above, runs with 1000 electrons with surplus energies near the transmission edge from −0.5 eV to 0.5 eV were simulated. The resulting output files were analyzed, by counting the transmitted electrons, which resulted in the following transmission functions:

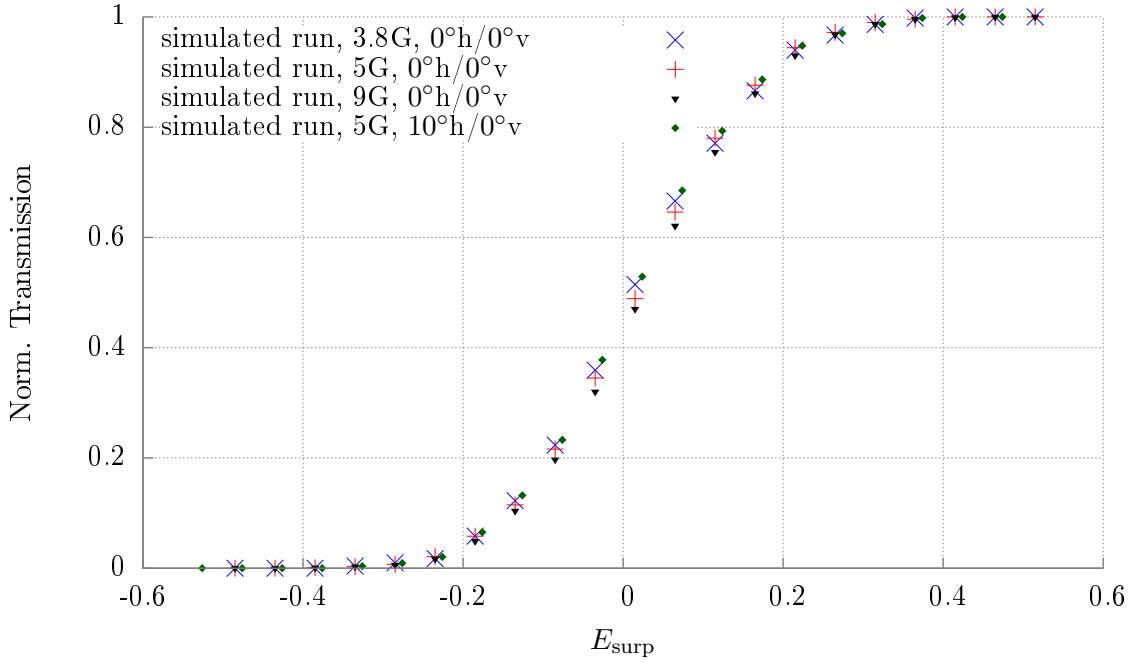

Figure 11: Simulated transmission curves for $U_{\mathrm{ie}} = 200\,\mathrm{eV}$, three different aircoil settings (3.8 G, 5 G, 9 G) at 0°h/0°v manipulator setting, and the 5 G setting for 10°h/0°v manipulator angle

It can be seen that the transmission function is centered about $E_{\mathrm{surp}} = 0\,\mathrm{eV}$, and starts at about $-0.3\,\mathrm{eV}$, which meets the expectation, as the relatively sharp transmission edge of the spectrometer is widened by the Gaussian energy distribution of the source, which was set to $\sigma = 0.134\,\mathrm{eV}$. Furthermore, the different aircoil settings do not have an notable influence on the transmission function, as they only vary the width of the spectrometer energy resolution $\Delta E_{\mathrm{mainspec}}$ such that $\Delta E_{\mathrm{egun}} \gg \Delta E_{\mathrm{mainspec}}$ still holds true. In 12, the simulation run with 5 G is compared to the equivalent experimental run M3.A5, run 5139:

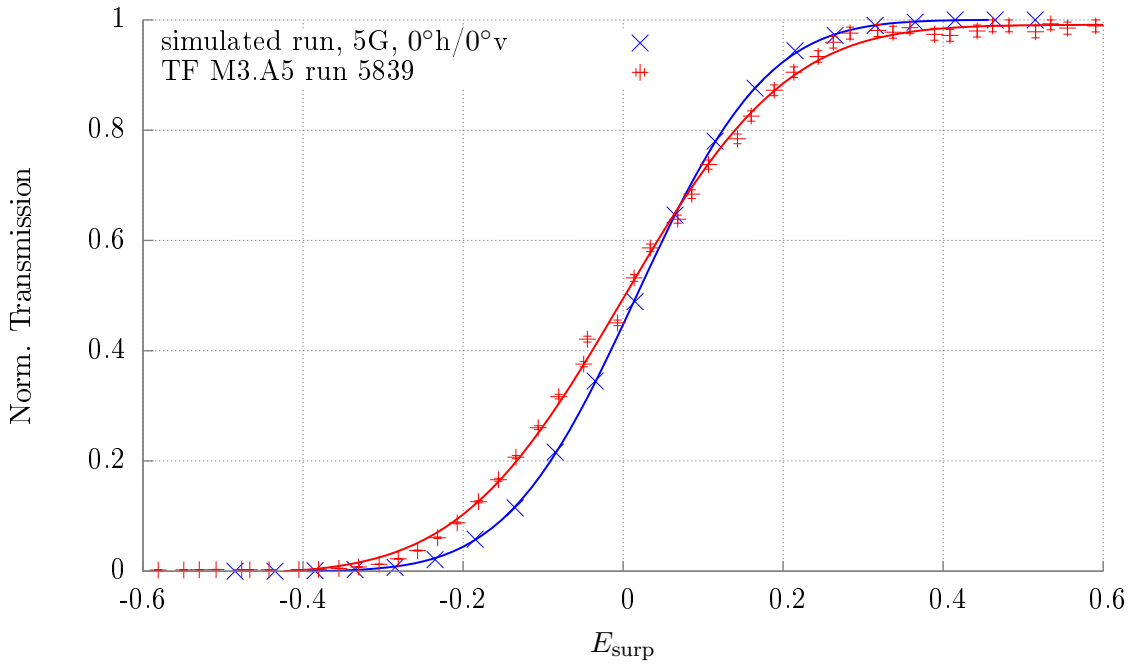

Figure 12: Comparison of the transmission function from M3.A5, run 5139 and the simulated run.

A transmission function

$$\mathrm{T}(E_{\text{surp}}) = 1 + \operatorname{erf}\left(\frac{1}{\sqrt{2}\sigma} E_{\text{surp}} - \Delta E\right)$$

was fitted to both the simulated and the experimental run data, giving $\sigma = 0.128(1)\,\text{eV}$ (simulation) respectively $\sigma = 0.163(3)\,\text{eV}$, which confirms the experimental observation described in the previous chapter, that the transmission function should be driven by the energy distribution of the starting electrons. The experimental data were shifted along the energy axis, such that the fit parameter ΔE is zero, because there is a constant energy offset as described in section 5.1

5.3.2 Time of flight

To obtain time of flight curves, the same settings as before were used, but using less fine energy steps (because the TOF curve is flatter than the transmission function) up to surplus energies of about 50 eV. Just as done with the experimental data, TOF spectra were created from the simulation output, and analyzed by fitting an asymmetric Gauß function

$$N(t) = a \exp\left(-\frac{(t-\tau)^2}{2\sigma^2}\right) \quad \text{with } \sigma = \begin{cases} \sigma_{\text{l}} & t < \tau \\ \sigma_{\text{r}} & t > \tau \end{cases}$$

with two different σ_i and a and τ as fitting parameters. This way a mean value τ for the time of flight could be determined for each spectrum. In the following figures, example spectra for low and high surplus energies of a simulated TOF run and run 6157 are shown.

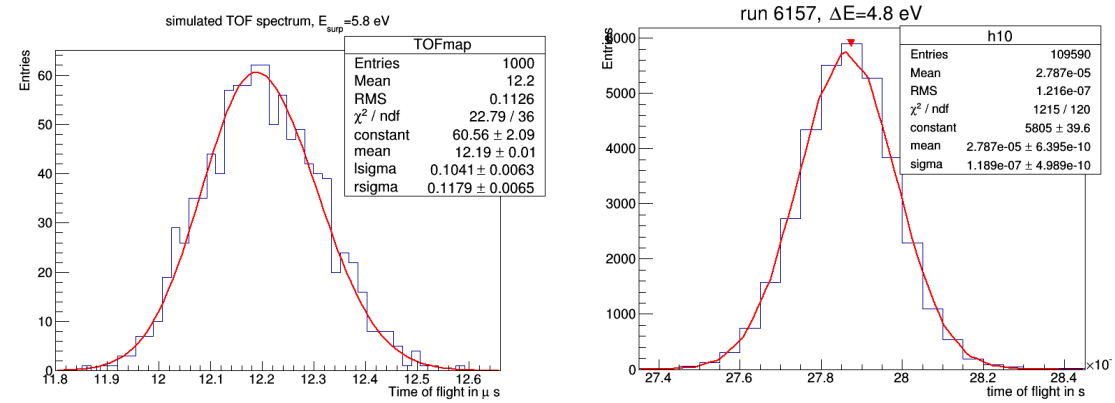

Figure 13: TOF spectra of simulation and experiment (run 6157) for low surplus energy.

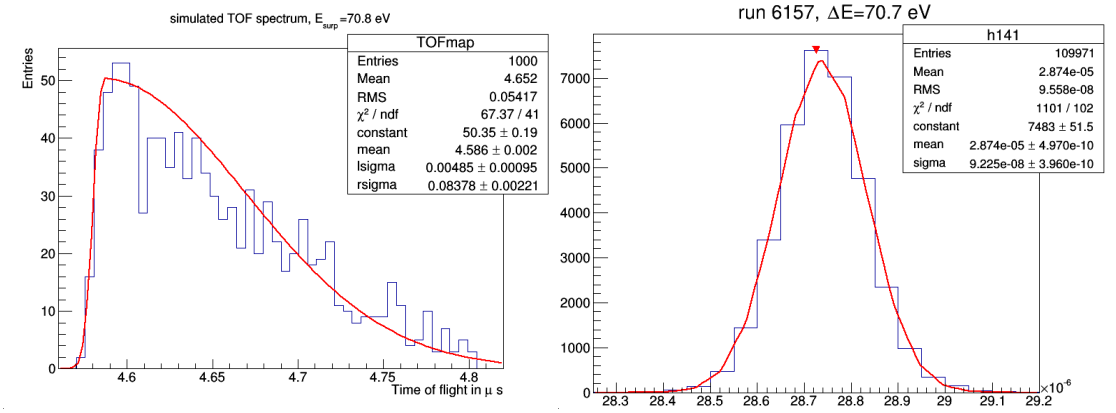

Figure 14: TOF spectra of simulation and experiment (run 6157) for high surplus energy.

For a surplus energy of about 5 eV, simulated and experimental spectra are both symmetric with $\sigma \approx 0.1\,\mu$s, but for a surplus energy of about 71 eV, the simulated spectrum becomes highly asymmetric, whereas the experimental spectrum stays symmetric. In order to examine this effect, the time of flight of two runs, with a surplus energy of 1 eV and 101 eV was plotted against the starting polar angle in figure 15.

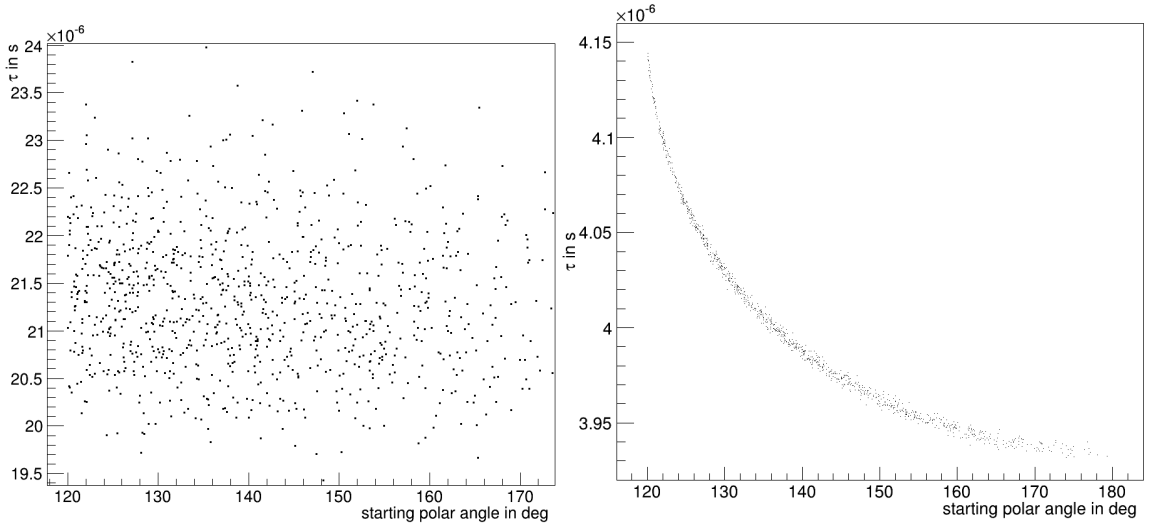

Figure 15: Time of flight as a function of starting polar angle for low (1 eV) and high (101 eV) surplus energy.

The time of flight is nearly independent of the starting angle in the first case, but becomes highly correlated with the starting angle for high surplus energies. The reason for is, that at low surplus energies and therefore high TOF values, the energy line width dominates and no angular dependency can be seen, whereas for higher surplus energies the influence of the line width decreases.

This should however not affect the time of flight curves much, as both σ_i are still multiple magnitudes smaller than τ. The fitted time of flight τ of each simulated spectrum was plotted against the surplus energy, together with the time of flight curve of the M4 run 6157 in figure 16.

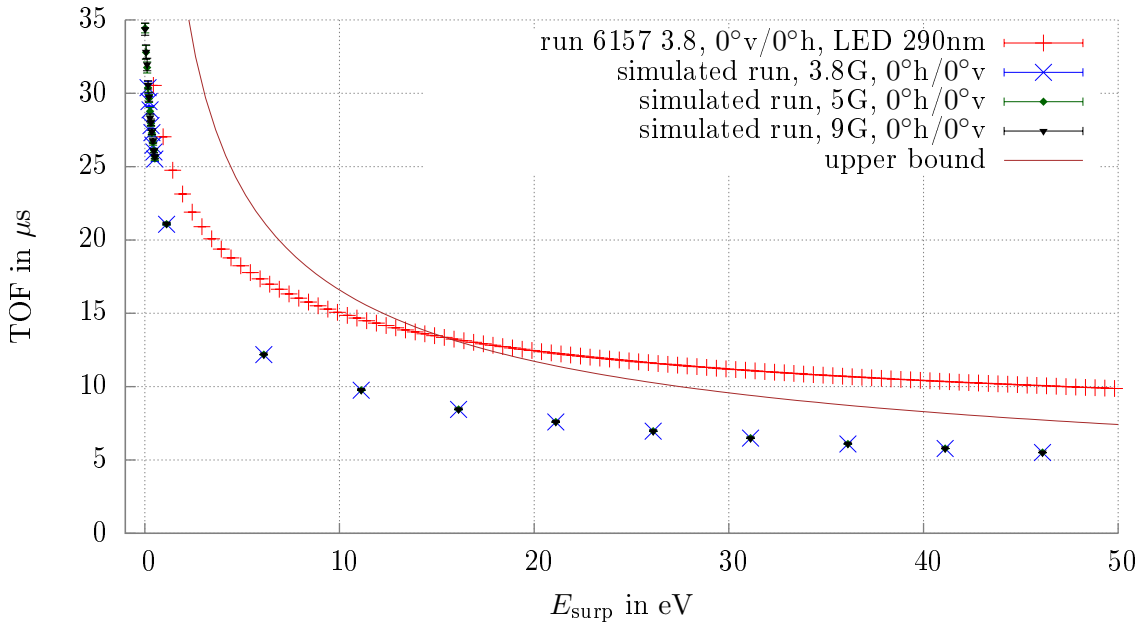

Figure 16: Simulated time of flight curves and the experimental one from M4 run 6157. There is a high discrepancy between the simulation and the experimental data.

The resulting time of flight curves are almost identical, but they do not fit the data of run 6157 at all and have an offset of about $5\,\mu$s. For a consistency check, the following estimation can be done: The minimum kinetic energy of an electron running against the spectrometer potential barrier is E_{surp}, this is the kinetic energy in the analyzing plane, therefore $E_{\text{kin}} \leq E_{\text{surp}}$. Energy conservation

$$E_{\text{surp}} = \frac{1}{2}mv^2$$

therefore defines an lower bound for the electron speed:

$$v \geq \sqrt{\frac{2E_{\text{surp}}}{m}}\,.$$

As the electron has to travel through the spectrometer, which is about $l = 24.4\,\text{m}$ long, its minimum time of flight can be

$$\tau_{\text{up}} = \frac{l}{v} \leq l\sqrt{\frac{m}{2E_{\text{surp}}}})\,.$$

This upper bound $\tau_{\text{up}}(E_{\text{surp}})$ was plotted in figure 16 and shows, that the experimentally obtained curve cannot be correct, but the plot suggests, that there might be a constant

offset between simulation and experimental curves. Therefore the same plot was created, but with a constant time offset of $\Delta\tau$=4.5 μs and surplus energy offset of $\Delta E = 1.1\,\mathrm{eV}$:

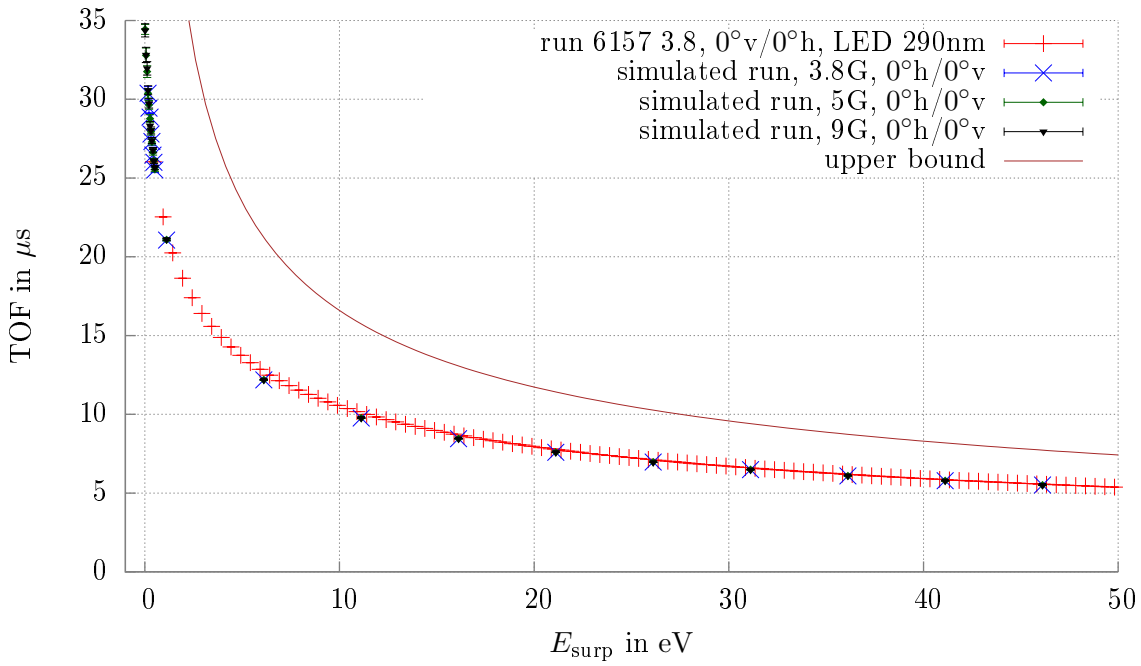

Figure 17: Time of flight curves as in figure 16, but a constant time offset of $\Delta\tau$=4.5 μs was subtracted from the experimental time of flights.

It can be seen that this way, the time of flight curves fit together very well. This would mean that there is a unknown delay in the experimental setup, that is responsible for this offset.

To verify this finding and to judge the quality of the simulation, the potential along the flight path of the tracked electrons was analyzed. Surprisingly, it showed an overshoot over 0 V in the starting- and end region at $z \approx \pm 11.6\,\mathrm{m}$, which is not physically allowed, since all voltages that were applied to the spectrometer are negative or zero. This issue was investigated, and it was found, that there is a bug in the elcd32 code, when calculating potentials with the zonal harmonic approximation. Therefore the potential for the same setting was calculated with the KEMField zonal harmonic solver, but here the issue was the same. Lastly, the KEMField direct solver was tested, and with this solver, the potential did not show the unphysical overshoot. A comparison of the potentials is shown in figure 18:

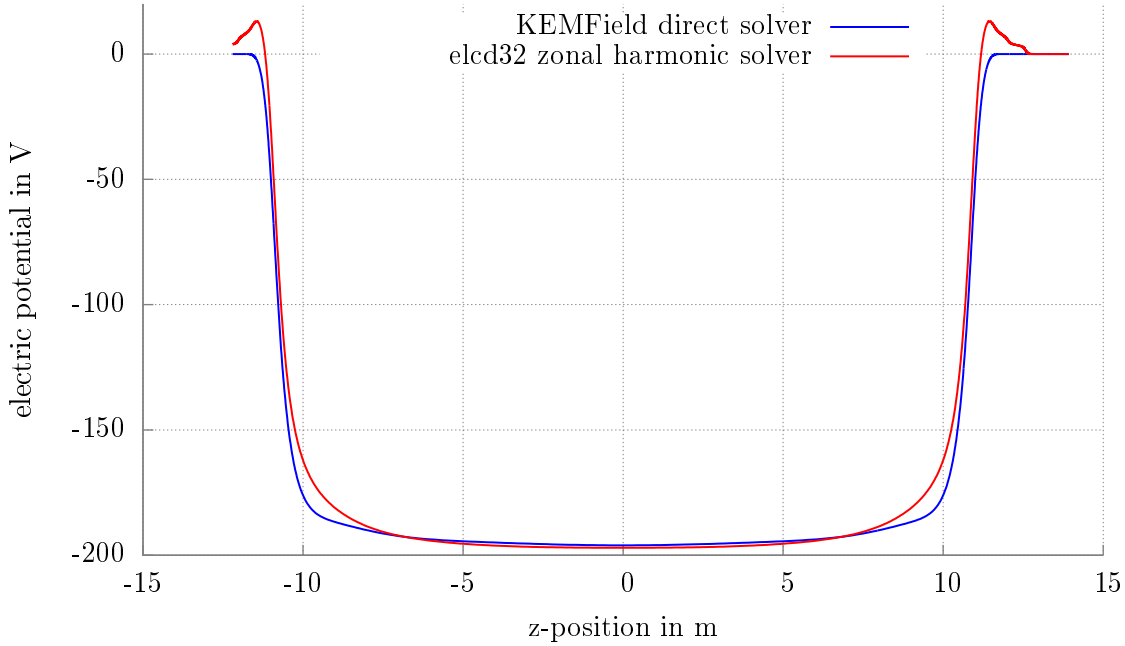

Figure 18: Potential of the KATRIN main spectrometer, with tank vessels at ground potential and the inner electrodes at $U_{\mathrm{ie}} = -200\,\mathrm{eV}$. When calculated with a zonal harmonic solver, the potential shows an unphysical overshoot, whereas the potential calculated by the direct solver is physically plausible. There seems to be a general problem concerning the zonal harmonic solvers in Kassiopeia. Therefore simulations with the KEMField direct solver were performed

Though the experimental time of flight curve in 16 cannot be correct and subtracting a time offset would make it fit the simulation, the simulation had to be rechecked nevertheless. Unfortunately, as mentioned in section 5.2, the KEMField solver is multiple magnitudes slower than the previously used elcd32 solver, allowing only single particle tracks in a reasonable amount of time. Accordingly, simulation runs with the corrected potential, but a single electron starting from the source were done, and compared to the original runs:

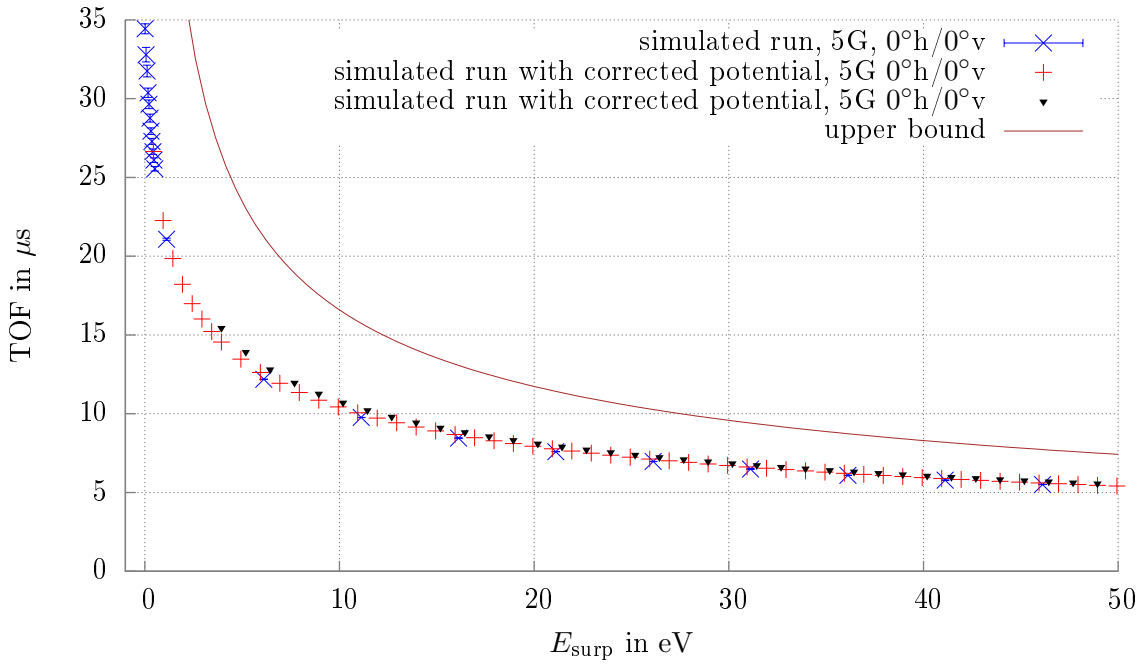

Figure 19: Comparison of simulation done with the wrong potential from figure 18, but with 1000 tracks, and single track simulation (due to high runtime) with the corrected potential. Obviously, both simulations deliver very similar results.

These results show that the time of flight curves do not change much between the two simulations, suggesting that the defect in the potential does not affect the time of flight significantly, and therefore the results can be trusted.

6 Summary and conclusion

In this thesis, the transmission and time of flight properties of the KATRIN main spectrometer were simulated using the Kassiopeia toolkit. The simulations, that were done with 1000 particles with a Gaussian energy and uniform angular distribution showed that the transmission function of the spectrometer does not change with different settings for the aircoils (defining the magnetic field B_{min} in the analyzing plane) and the manipulator. The comparison with the experimentally obtained transmission function showed good agreement.

The same cannot be said with regard to the time of flight, as here the simulations showed a significant discrepancy to the experimental data. A theoretical estimation yielding an upper bound $\tau_{\mathrm{up}}(E_{\mathrm{surp}})$ for the time of flight showed that the latter cannot be the correct as it violates this bound. Therefore the data were replotted with constant offsets of $\Delta\tau$=4.5 μs and $\Delta E = 1.1\,\mathrm{eV}$, in which the simulation fit well to the data.

Still, the simulations were further investigated by plotting the potential along the electron flight path. Surprisingly, the potential used for the simulation showed unphysical overshoots at the edges. Using different field computation however, it could be shown that this did not affect the time of flight significantly, therefore the results of this thesis point to the assumption, that there is a unphysical offset of $\Delta\tau$=4.5 μs in the experimental setup for KATRIN time of flight measurements, which might for instance be caused by delays in the DAQ system. Further investigation should be done to verify this findings and review the problem in field computation with Kassiopeia, as this was not possible in the time frame of this thesis.

References

[Be12] Jan D. Behrens, Simulations of stored electrons in the Penning trap between the KATRIN spectrometers, Institut fr Kernphysik, Westfälische Wilhelms-Universität Münster, 2012

[Bea80] G. Beamson et al. , J. Phys. Sci. Instrum. Vol. 13 (1980) 64

[KAT04] The KATRIN collaboration, KATRIN Design Report 2004, FZKA Scientific Report 7090

[M313] KATRIN internal document, M3 - E-gun Characteristics, version 0.9

[Hug10] K. Hugenberg , An angular resolved pulsed UV LED photoelectron source for KATRIN, Progress in Particle and Nuclear Physics , 2010

[SDS13] Various KATRIN internal *elog* entries, The Electronic Logbook for SDS commissioning measurements, `https://neutrino.ikp.kit.edu:8080/SDS-Measurements/`,

[Hug08] K. Hugenberg, *Diploma thesis*, Institut für Kernphysik, Westfälische Wilhelms-Universität Münster, 2008

[TOF13] Christian Weinheimer, Nicholas Steinbrink, et al., Neutrino mass sensitivity by MAC-E-Filter based time-of-flight spectroscopy with the example of KATRIN, arXiv:1308.0532, 2013

[RH06] Predrag Lazic, Hrvoje Stefancic and Hrvoje Abraham, The Robin Hood method - A new view on differential equations, Journal of Computational Physics 213 (2006) 117–140.

[Wol08] I. Wolff, Diploma thesis, Institut für Kernphysik, Westfälische Wilhelms-Universität Münster, 2008